RSC Advances

PAPER

View Article Online
View Journal | View Issue

Cite this: *RSC Adv.*, 2014, **4**, 60776

Cytotoxicity of silver(I), gold(I) and gold(III) complexes of a pyridine wingtip substituted annelated N-heterocyclic carbene†

Joydev Dinda,§*[ac] Abhishek Nandy,‡[b] Bidyut Kumar Rana,‡[c] Valerio Bertolasi,[d] Krishna Das Saha*[b] and Christopher W. Bielawski[ef]

Received 1st September 2014
Accepted 27th October 2014

DOI: 10.1039/c4ra09591j

www.rsc.org/advances

Starting from the proligand 1-methyl-2-pyridin-2-yl-2*H*-imidazo[1,5-*a*]pyridin-4-ylium chloride (**1**·HCl), three novel complexes [Ag(**1**)Cl] (**2**), [Au(**1**)Cl] (**3**) and [Au(**1**)Cl_3] (**4**) were synthesized and characterized using various spectroscopic techniques. In addition, the structure of **2** was elucidated using single crystal X-ray diffraction analysis, which revealed that the carbene nucleus and the chloride ion bound to the silver(I) were nearly linear (165.37(9)°). The gold(I)–NHC complex **3** was synthesized *via* transmetallation from the aforementioned silver complex **2**. Similarly, treatment of **3** with Au(SMe_2)Cl afforded **4**, ostensibly *via* a disproportionation process. The cytotoxicities of complexes **2**, **3**, and **4** were examined against HepG2 (human hepatocellular carcinoma), HCT 116 (human colorectal carcinoma), A549 (human lung adenocarcinoma), and MCF-7 (human breast adenocarcinoma) cells. Au(I)–NHC complex **3** exhibited a cytotoxicity that was similar to that of cisplatin towards all the four cancer cell lines tested; by comparison, Ag(I) NHC complex **2** and Au(III) NHC complex **4** appeared relatively less potent. Complex **3** was found to induce apoptosis in HepG2 cells.

1. Introduction

N-Heterocyclic carbenes (NHCs) are an established class of ligands for a broad range of transition metals, and are relatively easy to synthesize, tune, and modify.[1,2] Due to their strong σ-donating and weak π-accepting properties, NHCs often form stable organometallic complexes with metals in different oxidation states.[3,4] Currently, many researchers in this field are focusing on three main directions: (i) the development of novel NHC ligands,[2,5] (ii) applications of NHCs in catalysis and materials science,[6,7] and (iii) the use of NHCs in biomedical applications.[8–14] One of the first reports of the biological activities of metal–NHC complexes was published in 1996 by Cetinkaya *et al.*, who disclosed the antibacterial properties of various NHC-containing ruthenium(II) complexes.[13] Afterwards, the number of reports on metal–NHC complexes in various biomedical applications steadily increased, and currently, this is one of the most active research areas within the field of bioinorganic chemistry.[8–14] In particular, the development of metal-based drugs for the treatment of cancer or infectious diseases has been a focal point, as has the biological screening and evaluation of metal–NHC complexes.

Over the past decade, a broad range of silver(I) complexes supported by NHCs has been synthesized[15,16] and explored for potentially useful photophysical properties[16–18] as well as intermediates for accessing other types of metal complexes.[19] More recently, Ag(I)–NHC complexes were found to be potent agents against drug-resistant pathogens.[20–22] Indeed, recent studies by Youngs and others have shown that Ag–NHCs are useful in antibacterial and anticancer applications.[20,21] Most silver complexes appear to display similar modes of action, particularly *via* the release of Ag^+ ions that enter cell membranes and disrupt their functions. However, an ongoing challenge with most Ag-based drugs is that they quickly lose their effectiveness due to the rapid release of the Ag^+ ions. It is envisioned that this limitation may be overcome through the use of NHCs, as these ligands tend to bind strongly to metals.[8]

[a]*Department of Chemistry, ITM University-Gwalior, Gwalior-474001, M.P., India. E-mail: dindajoy@yahoo.com; Fax: +91-751-2440058; Tel: +91-751-2438539*

[b]*Cancer Biology and Inflammatory Disorder Division, CSIR-Indian Institute of Chemical Biology, Jadavpur, Kolkata-700032, West Bengal, India. E-mail: krishna@iicb.res.in; Tel: +91-943258483*

[c]*School of Applied Science, Applied Synthetic Chemical Research Laboratory, Haldia Institute of Technology, Haldia-721657, Purba Medinipur, West Bengal, India*

[d]*Dipartimento di Chimica and Centro di Strutturistica Diffrattometrica, Universita' di Ferrara, Via L. Borsari, 46, Italy*

[e]*Department of Chemistry, University of Texas at Austin, 1 University Station, A1590, Austin, TX 78712, USA*

[f]*Department of Chemistry, Ulsan National Institute of Science and Technology (UNIST), Ulsan, 689-798, Korea*

† Electronic supplementary information (ESI) available. CCDC 982347. For ESI and crystallographic data in CIF or other electronic format see DOI: 10.1039/c4ra09591j

‡ Abhishek Nandy and Bidyut Kumar Rana equally contributed to this work.

§ Present address: Department of Chemistry, ITM University-Gwalior (M.P.), India.

Besides silver, other precious metals have also found utility in biomedical applications. Gold is a notable example, as it has been used for centuries in various Chinese medicines. More recently, precious metals have been investigated for their activities against tuberculosis and arthritis. For example, Ridaura (auranofin/triethyl-phosphine gold(I) tetraacetatothioglucose), Myocrisin (sodium aurothiomalate), and Solganal (aurothioglucose) are commercially available and are being clinically utilized.[23] The gold(I) phosphine complex auranofin, which was initially developed as an anti-rheumatic agent, was shown to have potential use as an anticancer agent.[24] Unfortunately, auranofin is readily metabolized by reaction with natural thiols, which significantly restricts its activity.[25] To increase the stability of gold complexes under biologically relevant conditions, attention has been directed toward the synthesis and study of analogous complexes bearing stabilizing NHC ligands.[26] Berners-Price and Barnard obtained excellent results against mouse cancer cells using a Au(I)–NHC complex.[27] Panda and Ghosh also successfully developed a Au(I)–NHC complex that exhibited excellent efficiency against HeLa cell proliferation.[28] In parallel, Au(I)–NHC complexes were reported by Berners-Price to display selective mitochondrial targeting and selective thioredoxin reductase inhibition characteristics. Filipovska *et al.* established a new approach to mitochondria-targeted antitumor agents using Au(I)–N-heterocyclic carbene compounds, where selective mitochondria targeting and selective thioredoxin reductase inhibition properties were achieved using a single molecular species.[27,29,30] From a general design perspective, a detailed structure–activity relationship study revealed that the inhibitory potency of Au(I)–NHC complexes may be increased through the incorporation of chloride ligands as opposed to the use of two NHCs.[31]

Although the biological applications of gold and gold(I) complexes are broad, there are relatively few analogous Au(III) complexes described in the literature. The paucity of examples is surprising, as their relatively high electrophilicity may result in compounds that display enhanced biological activities under analogous conditions.[22] Since Au(III) is isoelectronic with Pt(II) and both metals would be expected to form complexes with square planar geometries, one may expect Au(III) complexes to display biological properties similar to those of cisplatin. Moreover, the challenges often encountered when using cisplatin, such as nephrotoxicity and other side effects,[32] may be minimized or eliminated through the use of appropriately designed Au(III)–NHC based agents.[33]

Recently, the chemical and biological properties of 2-phenylpyridine-supported Au complexes, particularly their cytotoxicity toward the MOLT-4 and other tumour cell lines, were reported.[34] In addition, the fluorescence and biological properties of Pt, Rh, Ir, and other complexes[35] of 2-phenylpyridine have attracted attention. Building on these results, we designed an analogous NHC ligand: 1-methyl-2-pyridin-2-yl-2*H*-imidazo[1,5-*a*]pyridin-4-ylium salt (see Charts 1 and 2). The aforementioned NHC was envisioned to (i) form robust complexes that are stable to ambient air and are moisture-stable and (ii) stabilize a broad range of metal complexes in various oxidation states. Herein, the cytotoxicities of various Ag(I), Au(I), and Au(III) complexes containing the aforementioned NHC were evaluated *in vitro* using a range of cancer cell lines. The cytotoxicity of the present gold(I) complex was compared with the cytotoxicity of a novel Au(I)–NHC complex against HeLa (human cervical carcinoma), HepG2 (human hepatocellular carcinoma), and B16F10 (mouse melanoma) cell lines.[36]

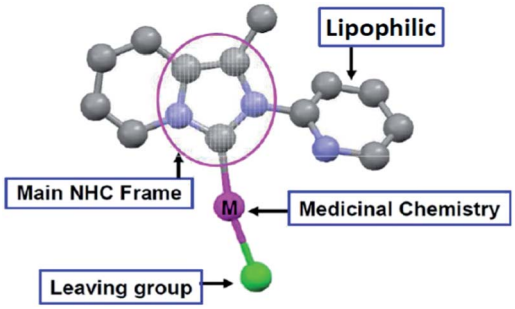

Chart 1 Key structural features of a novel class of NHC-based anticancer agents.

2. Results and discussion

2.1. Synthesis and characterization

The salt 1-methyl-2-pyridin-2-yl-2*H*-imidazo[1,5-*a*]pyridin-4-ylium chloride (**1·HCl**) was synthesized *via* formylative cyclization of the corresponding Schiff base 2-acetylpyridyl-*N*-(2-pyridine)methylamine using standard conditions as previously reported.[37] Imidazolium salts are common precursors to NHC ligands, and transfer of such derived ligands to group d^{10} metal complexes is often achieved *via* silver(I) complexes. Indeed, treatment of Ag_2O with **1·HCl** afforded the NHC–Ag(I)–Cl complex **2** (Scheme 1), as determined by the absence of the diagnostic ^{1}H NMR signal associated with the imidazolium precursor (δ = 10.62 ppm (s); DMSO-d_6). In addition, the ^{1}H NMR spectrum recorded for **2** revealed two doublets in the range of 8.68–8.47 ppm, which were assigned to the two α-protons (a and h mentioned in Scheme 1) associated with the pyridine component of the ligand. Although Ag–C coupling was not observed, a singlet was recorded at 172.4 ppm upon ^{13}C NMR spectroscopic analysis of a solution of **2** and was attributed to the carbene center. Additional structural support was obtained *via* mass spectrometry, which revealed a signal consistent with a $[Ag(1)]^+$ ion (m/z = 316.8), and single crystal X-ray crystallography. As shown in Fig. 1, the solid state structure of **2** revealed that the carbene center was coordinated to the Ag center with an average Ag(I)–C distance of 2.081(3) Å and an

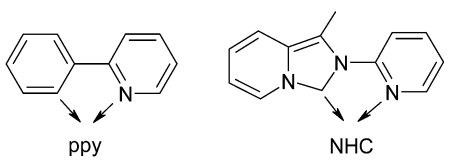

Chart 2 C, N donor ligands.

average Ag(I)–Cl distance of 2.3585(12) Å. Additional crystallographic details are summarized in Table 1 and discussed below.

NHC–Au(I)–Cl complex **3** was obtained *via* transmetalating **2** with $Au(SMe_2)Cl$.[19] Complex **3** was characterized by the diagnostic shifting of the N*C*HN component in ^{13}C NMR, as well as the observance of a general downfield shift for most of the aromatic protons as compared to the analogous signals recorded for **2**. Moreover, complex **3** displayed a ^{13}C NMR signal at 178.1 ppm and a *m*/*z* signal at 406.2, consistent with the formation of a $[Au(1)]^+$ ion.

Finally, following a disproportionation protocol that was previously reported by our group,[38] Au(III)–NHC complex **4** was synthesized using **3** and $Au(SMe_2)Cl$. Upon stirring a colorless acetonitrile solution of Au(I)–NHC complex **3** and $Au(SMe_2)Cl$ at room temperature for 6 h, an orange/yellow color formed, along with the appearance of a yellow precipitate of Au(0); the latter may be reconverted to $Au(SMe_2)Cl$. Following separation and purification, the yellow product was analyzed by NMR spectroscopy. Although the ^1H NMR spectrum of the isolated solid was similar to that recorded for complex **3**, the former displayed a relatively upfield ^{13}C NMR signal at $\delta = 162.6$ ppm, which was subsequently assigned to a $C_{carbene}$ atom coordinated to a Au(III) center. For comparison, the ^{13}C NMR resonance observed for the $C_{carbene}$ atom in the isolated material was slightly downfield with respect to the analogous N*C*HN signal recorded for the parent imidazolium salt (154.3 ppm)[37] and consistent with analogous signals displayed by $[AuX_3(NHC)]$ complexes bearing imidazolin-2-ylidene or imidazolidin-2-ylidene ligands.[39,40] The isolated material was further studied by mass spectrometry (ESI Fig. S1†), which revealed signals consistent with the formation of $[Au(1)Cl_2]^+$ (*m*/*z* of 477.2) and $[Au(1)Cl]^+$ (*m*/*z* of 441.7).

2.2. X-ray crystallography of complex 2

Single crystals suitable for X-ray diffraction were grown *via* the slow diffusion of diethyl ether into a dichloromethane solution saturated with **2**. As shown in Fig. 1, a nearly linear (165.37(9)°) $C_{carbene}$–Ag(I)–Cl bonding angle was observed. Moreover, the Ag–C distance (2.081(3) Å) was consistent with those measured in the solid state structures of other Ag–NHC complexes[16] and within the sum of van der Waals radii of the silver and carbon nuclei (2.111 Å). The N(1)–C(1)–N(2) bond angle was measured to be 103.4(3)°, which is shorter than that reported for a Hg(II)–NHC complex containing the same ligand (105.6(4)°).[37] As shown in Scheme 2, the molecular packing diagram of **2** revealed a dimeric structure that was supported by Ag–Cl···Ag–Cl and C–H···Cl interactions. Moreover, a combination of C–H···Cl and C–H···π interactions revealed stair-like and one-dimensional chain-like structures.

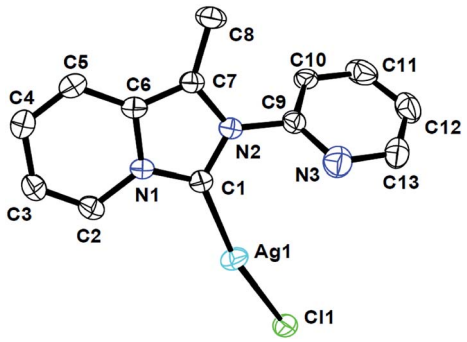

Fig. 1 Thermal ellipsoid plot (40% probability) of **2** (H atoms have been removed for clarity). Selected bond lengths (Å) and angles (deg): Ag(1)–C(1) = 2.081(3), Ag(1)–Cl(1) = 2.3585(12), N(2)–C(1) = 1.364(4), N(2)–C(7) = 1.383(4), C(1)–Ag(1)–Cl(1) = 165.37(9), N(1)–C(1)–N(2) = 103.4(3).

2.3. Cytotoxicity studies

The growth inhibitory effects of complexes **2**, **3**, and **4** were investigated against the HepG2, HCT 116, A549, and MCF-7 cell lines using MTT assays.[36] Treatment at different concentrations of complexes **2**, **3**, and **4** (*i.e.*, 0, 2.5, 5, 7.5, and 10 μM) reduced the viability of these cancer cells in a dose-dependent manner after 24 h. In general, complex **3** exhibited relatively high activity when compared to complex **2** or **4**. Moreover, when compared to complex **2**, **3**, or **4**, cisplatin, a commonly used anticancer drug, displayed a higher rate of growth inhibition of the above-mentioned cancer cell lines (Table 2 and Fig. 2). The cytotoxicities displayed by complexes **2–4** may be in part related to their lipophilicities, as well as to the chloride ligands.[36] For example, Gautier previously reported that the potencies displayed by various Ag–NHC complexes may depend upon the substituents appended to the imidazole ring, as well as the degree of saturation.[12] In general, the incorporation of bulkier substituents results in higher lipophilicities and ultimately increases cytotoxicities.[12] Moreover, the potency was found to increase when chloride or organophosphorous ligands were incorporated into the gold(I)–NHC complexes.[31] The use of chloride ligands has also been shown to aid the transport of Ru complexes into cells, due to the concentration gradient between the intra- and extracellular concentrations of chloride ions. The activated drug is thus formed upon chloride dissociation, as the process effectively creates a coordination site on metal that can bind with DNA.[41]

Berners-Price's group demonstrated that Au(I)–NHC complexes are potent inducers of mitochondrial membrane permeabilization (MMP) but less potent than auranofin.[42]

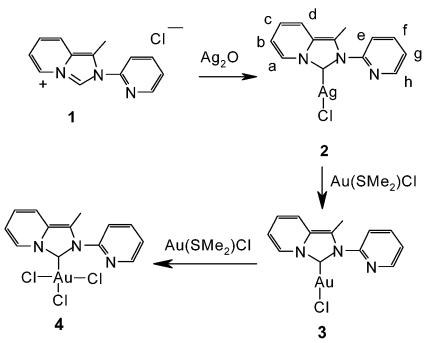

Scheme 1 Synthesis of various Ag(I), Au(I), and Au(III)–NHC complexes. The letters surrounding the structure of **2** refer to the NMR assignments; see the Experimental section.

Table 1 Crystal data and structural refinement parameters for complex **2**

	Complex (**2**)
Empirical formula	$C_{13}H_{11}AgClN_3$
Formula weight	352.57
Temperature (K)	293(2)
Wavelength (Å)	0.71073
Crystal system	Triclinic
Unit cell dimensions	
a (Å)	7.460(3)
b (Å)	9.046(4)
c (Å)	9.952(4)
α (°)	83.312(5)
β (°)	72.451(8)
γ (°)	87.187(8)
Volume (Å^3)	636.0(4)
Z	64
Calcd density (Mg m$^{-3)}$	2.669
Absorption coefficient (mm^{-1})	5.160
F(000)	468
Crystal size (mm)	0.21 × 0.17 × 0.14
θ range (°)	2.16–25.00
Limiting indices	$-8 \le h \le 8$, $-10 \le k \le 10$, $-11 \le l \le 11$
Reflections collected/unique data/R(int)	6012/2226/0.0259
Observed data/parameters	2101/164
Goodness-of-fit on F^2	1.068
Final R indices [$I > 2\sigma(I)$]	$R_1 = 0.0275$, w$R_2 = 0.0784$
R indices (all data)	$R_1 = 0.0291$, w$R_2 = 0.0796$

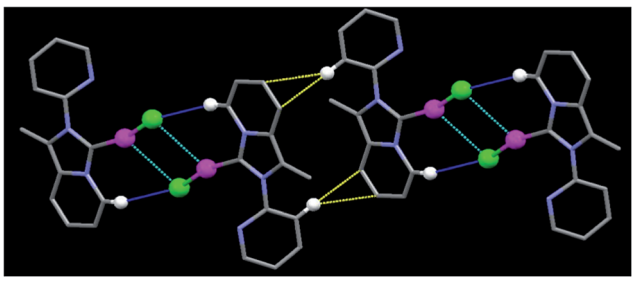

Scheme 2 Illustration of the Ag···Cl, C–H···π, and C–H···Cl interactions found in the solid state structure of **2**.

Table 2 IC_{50} (μM) of cancer cells in the presence of cisplatin or complex **2**, **3**, or **4** after 24 h[a]

Cells	Cisplatin	Complex **2**	Complex **3**	Complex **4**
HepG2	4.31 ± 1.10	7.57 ± 4.06	4.91 ± 3.6	7.01 ± 1.65
HCT-116	4.89 ± 2.29	5.67 ± 2.29	5.08 ± 3.8	5.98 ± 2.17
A549	6.12 ± 3.67	6.23 ± 1.49	5.23 ± 2.96	6.56 ± 1.42
MCF-7	4.42 ± 1.02	6.42 ± 0.78	5.18 ± 1.35	4.96 ± 1.43

[a] Cells were treated with different concentrations of cisplatin or complex **2**, **3**, or **4** ranging from 0 to 10 μM for 24 h, respectively. The IC_{50} values were calculated from MTT assays. The mean values are ± S.D and represent one of three representative experiments.

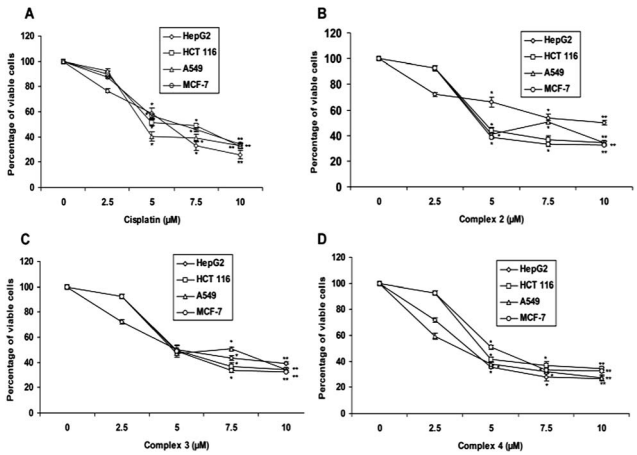

Fig. 2 Percentage viability curves of HepG2, HCT 116, A549, and MCF-7 cells following treatment for 24 h with: (A) cisplatin (0, 2.5, 5, 7.5, and 10 μM), (B) complex **2** (0, 2.5, 5, 7.5, and 10 μM), (C) complex **3** (0, 2.5, 5, 7.5, and 10 μM), or (D) complex **4** (0, 2.5, 5, 7.5, and 10 μM). Values are the mean ± S.D and represent one of the 3 representative experiments. *P < 0.05 and **P < 0.01.

Moreover, Raubenheimer *et al.* reported the cytotoxicity properties of a bis-ferrocenylated NHC–gold(I) complex toward HeLa and CoLo 320 cell lines.[43] However, complexes **2**, **3**, and **4** failed to display cytotoxic properties towards human peripheral mononuclear blood cells (hPBMCs), which was in accordance with earlier reports that indicated that there was low potency of growth inhibition displayed by Au(I) and Ag(I) complexes towards non-transformed cell lines, particularly with respect to cisplatin (Table 3).[44] The relatively low activity of Au(III)–NHC complex **4** may be explained by reduction of the central Au(III) to Au(I) upon interacting with intracellular thiols.[29,30]

Table 3 IC_{50} (μM) of cells in the presence of cisplatin or complex **2**, **3**, or **4** after 24 h in peripheral blood mononuclear cells (PBMCs)[a]

Cells	Cisplatin (μM)	Complex **2** (μM)	Complex **3** (μM)	Complex **4** (μM)
PBMCs	6.86 ± 2.31	>10	>10	>10

[a] Cells were treated with different concentrations of cisplatin, **2**, **3** or **4**, ranging from 0 to 10 μM, for 24 h. The corresponding IC_{50} values were calculated from an MTT assay. The values reported in the table are the mean ± standard deviation (S.D.) and represent one of three representative experiments.

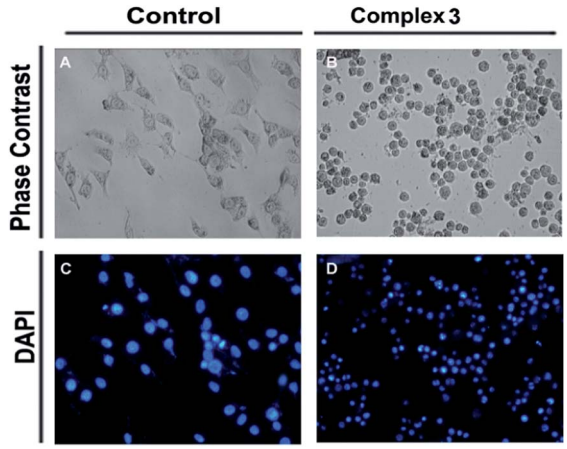

Fig. 3 Morphological changes of the DAPI-stained HepG2 cells treated with complex **3** (IC_{50} concentration) after 24 h. (A–C) Phase contrast and DAPI images of vehicle-treated cells. (B–D) Cells treated with complex **3** at a pre-determined IC_{50} concentration after 24 h. Magnification at 20×.

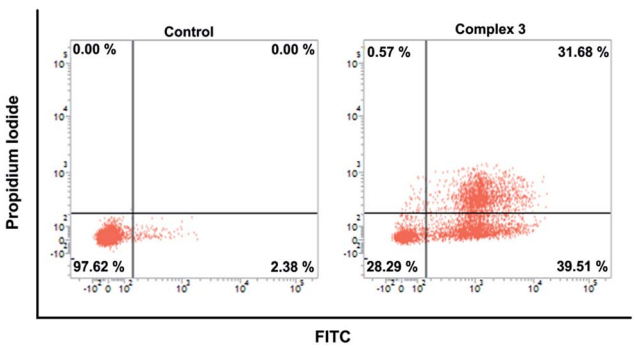

Fig. 4 Flow cytometry analysis of apoptosis induction of HepG2 cells after treatment with complex **3** (IC_{50} concentration) for 24 h.

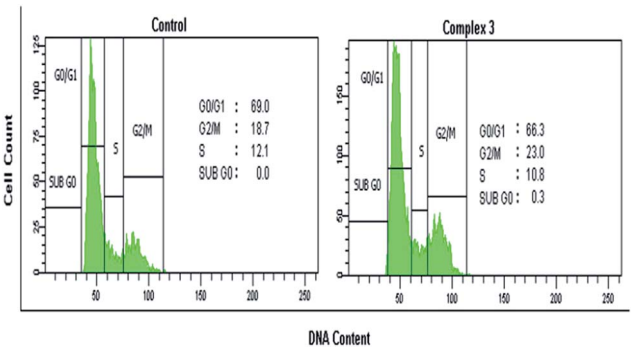

Fig. 5 Cell cycle analysis of HepG2 cells treated with complex **3** at a pre-determined IC_{50} concentration for 24 h.

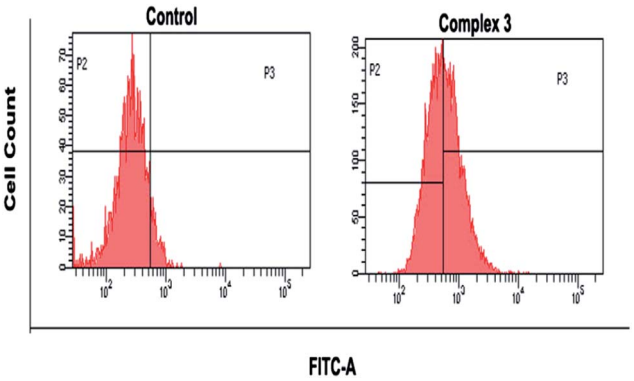

Fig. 6 Flow cytometry analysis of cellular ROS generation after treatment for 24 h with complex **3** at a pre-determined IC_{50} concentration.

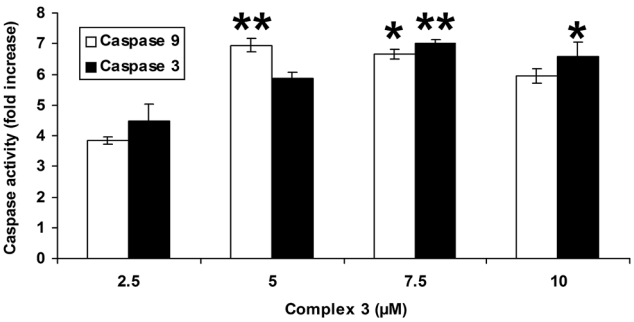

Fig. 7 Changes in caspase-9 and caspase-3 activity following treatment of HepG2 cells with complex **3** (0, 2.5, 5, 7.5, and 10 μM) for 24 h, as determined by a colorimetric caspase assay kit. Values are the mean ± S.D and represent one of the 3 representative experiments. *$P < 0.05$ and **$P < 0.01$.

2.4. Induction of apoptosis by complex 3

Complex **3** showed a higher cytotoxicity toward the HepG2 cell line as compared to the other cancer cell lines tested in this study. As such, the potential role of complex **3** in the induction of apoptosis in HepG2 cells was further investigated. After 24 h, complex **3** induced characteristic apoptotic changes in morphology, including cell shrinkage, rounding, chromatin condensation, and DNA fragmentation, upon staining with 4′,6-diamidino-2-phenylindole (DAPI) (Fig. 3).

Phosphatidylserine (PS) externalization from the inner cell membrane to the outer membrane is a prerequisite step of apoptosis, as externalized PS can bind with annexin V.[45] After 24 h of treatment with complex **3** at a pre-determined IC_{50} concentration, the percentage of apoptotic cells was measured

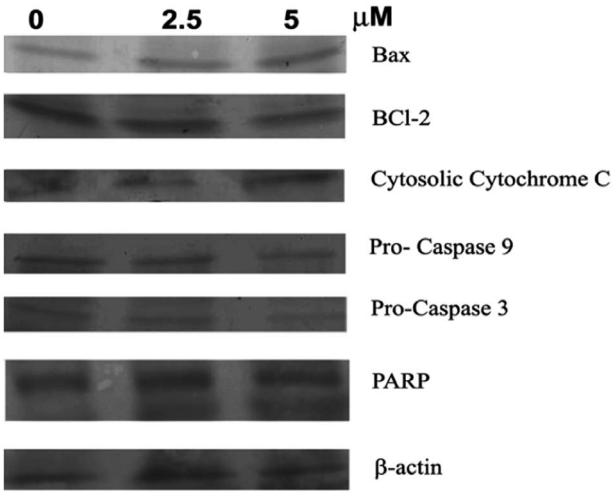

Fig. 8 Expression of various pro- and anti-apoptotic proteins following treatment of HepG2 cells with complex **3** (0, 2.5, and 5 μM) for 24 h with β-actin as a loading control.

to be 71.19%, significantly higher than that measured in the vehicle-treated cells (2.38%) (Fig. 4). Collectively, these findings suggested to us that complex **3** induced the apoptosis of HepG2 cells in a manner similar to that of previously reported Au(I)–NHC complexes.[46]

2.5. Induction of cell cycle arrest by complex 3

It is known that apoptosis is preceded by cell cycle arrest at various phases of cell division.[47] Treatment of HepG2 cells with complex **3** at a predetermined IC_{50} concentration for 24 h showed a gradual increase in the number of cells in G2/M phase (Fig. 5). The percentage of G0/G1 population of HepG2 cells treated with complex **3** at a pre-determined IC_{50} concentration (IC_{50} concentration) of treated HepG2 cells for 24 h was measured to be 69.0% and 66.3%, respectively, revealing a decrease in the cell population in the G0/G1 phase upon treatment with complex **3**. In contrast, the percentage of G2/M population of HepG2 cells treated with complex **3** at a pre-determined IC_{50} concentration was 18.7% and 23.0% respectively, indicating that complex **2** may mediate cell cycle arrest at the G2/M phase. Collectively, these results suggested to us that complex **3** induced apoptosis in HepG2 cells and may inhibit the cell cycle at the G2/M phase.

2.6. Complex 3-induced apoptosis of HepG2 cells involves an increase in ROS generation

In accord with previous reports,[48,49] the treatment of HepG2 cells with complex **3** at a pre-determined IC_{50} concentration for 24 h led to ROS generation, with a FITC mean at 305 (for vehicle-treated cells) and 703 for complex **3** (IC_{50} concentration). This indicated a shift in ROS generation from the vehicle-treated cells to those treated with complex **3**, thereby indicating that apoptosis of HepG2 cells by complex **3** also involves ROS generation (Fig. 6).

2.7. Complex 3-mediated apoptosis of HepG2 cells proceeds *via* the mitochondrial death pathway

Treatment of HepG2 with complex **3** at various concentrations (*i.e.*, 0, 2.5, 5, 7.5, and 10 μM) for 24 h led to an increase in the caspase-9 as well as in the caspase-3 activity (Fig. 7). Based on these observations, we believe that complex **3**-mediated apoptosis in HepG2 cells may occur *via* a mitochondrial death pathway[11] that is accompanied by the expression of the aforementioned caspases.[48,49]

2.8. Complex 3-mediated apoptosis of HepG2 cells involves an increase in the expression of apoptotic proteins

Previous reports have indicated increased expression of various apoptotic proteins upon treatment of cancer cells with Au(I)–NHC complexes.[48,49] Treatment with HepG2 cells with complex **3** at various concentrations (*i.e.*, 0, 2.5, and 5 μM) for 24 h led to increased expression of Bax, decreased expression of BCl-2, and downregulation of procaspase-9 and -3, with increased levels of cytosolic cytochrome c leading to increased PARP cleavage (Fig. 8). Thus, complex **3** appeared to mediate cell death by involving apoptotic proteins that participate in the mitochondrial death pathway.

3. Conclusion

In summary, we have synthesized and characterized novel Ag(I), Au(I), and Au(III) complexes supported by an NHC ligand, and explored the cytotoxicities of these complexes against cancer cells, including HepG2, HCT 116, MCF-7, and A549. Au(I)–NHC complex **3** showed the highest growth inhibitory effect towards HepG2, which may be due to the unique combination of lipophilicity and stability displayed by this complex.

4. Experimental section

4.1. General considerations

The following reagents were purchased from Sigma-Aldrich and used without further purification: 2-acetylpyridine, 2-aminopyridine, Ag_2O, and paraformaldehyde. The complex $Au(SMe_2)Cl$ was prepared according to a previously published procedure.[50] Unless otherwise noted, all manipulations were carried out under ambient conditions. All solvents were distilled over the appropriate drying agents and purged with nitrogen prior to use. NMR spectra were measured on Bruker 300 MHz and 100.5 MHz spectrometers for ^1H NMR and ^{13}C NMR experiments, respectively, at 25 °C using tetramethylsilane as an internal standard. Elemental analyses were performed with a Perkin-Elmer Analyzer model 2400 (CHN).

4.1.1. Synthesis of 1-methyl-2-pyridin-2-yl-2*H*-imidazo[1,5-*a*]pyridin-4-ylium chloride (1). A mixture of 2-pyridyl-*N*-(2-acetylpyridyl)methylamine (1000 mg, 5.1 mmol), 2 drops of formic acid, triethylorthoformate (0.5 mL), crushed 91% paraformaldehyde powder (153 mg, 5.1 mmol), and dioxane (20 mL) was stirred at room temperature for 8 h. The resulting suspension was then heated to reflux for an additional 2 h. Afterwards, 2 N HCl in diethyl ether (5 mL) was added dropwise to the

mixture, which resulted in the formation of a light yellow aqueous layer. After stirring for another 2 h, the aqueous layer was separated using a separatory funnel. The organic phase was diluted with methanol (20 mL) and then filtered to remove unreacted paraformaldehyde. Subsequent removal of the residual volatiles under reduced pressure afforded the desired product as a light yellow viscous oil (776 mg, 3.16 mmol, 62% yield). ^{1}H NMR (DMSO-d_6, 300 Mz, 25 °C): δ 10.62 (s, 1H, N*CH*N), 8.82 (d, J = 4.54 Hz, 1H, H^a), 8.56 (d, J = 7.20 Hz, 1H, H^e), 8.32 (t, J = 7.63 Hz, 1H, H^i), 8.21 (d, J = 7.68 Hz, 1H, H^d), 7.86 (t, J = 7.64 Hz, 1H, H^c), 6.93 (t, J = 7.71 Hz, 1H, H^f), 6.84 (t, J = 6.80 Hz, 1H, H^h), 2.14 (s, 3H, H^g). ^{13}C NMR (DMSO-d_6, 100.5 MHz, 25 °C): δ: 154.3, 147.6, 141.4, 127.7, 127.1, 126.7, 124.6, 124.4, 122.3, 121.1, 119.3, 119.0, 12.2. MS (FAB+): m/z 210.0 (M^+ − Cl).

4.1.2. Preparation of NHC–Ag–Cl complex 2. A mixture of proligand 1 (250 mg, 1.02 mmol), silver oxide (122.7 mg, 0.53 mmol), and dichloromethane (20 mL) in the presence of molecular sieves was stirred in the dark at room temperature for 4 h. The resulting mixture was filtered through a plug of celite to remove unreacted Ag_2O. Subsequent removal of the residual solvent under reduced pressure afforded the desired complex as a white solid (233.6 mg, 0.66 mmol, 65% yield). ^{1}H NMR (DMSO-d_6, 300 MHz, 25 °C): δ 8.68 (d, J = 4.53 Hz, 1H, H^a), 8.47 (d, J = 7.21 Hz, 1H, H^e), 8.13 (t, J = 7.66 Hz, 1H, H^i), 7.86 (d, J = 7.7 Hz, 1H, H^d), 7.66 (t, J = 7.66 Hz, 1H, H^c), 6.96 (t, J = 7.83 Hz, 1H, H^f), 6.82 (t, J = 6.80 Hz, 1H, H^h), 2.13 (s, 3H, H^g). ^{13}C NMR (DMSO-d_6, 100.5 MHz, 25 °C): δ 172.4, 154.8, 152.2, 137.6, 137.4, 127.6, 126.9, 124.1, 122.7, 120.8, 118.2, 118, 12.3. Anal. calcd for $C_{13}H_{11}N_3AgCl$: C, 44.28; H, 3.12; N, 11.92%. Found: C, 44.19; H, 3.13; N, 11.83%.

4.1.3. Preparation of NHC–Au–Cl complex 3. After stirring a mixture of silver(I)–NHC complex **2** (120 mg, 0.34 mmol) and dichloromethane (15 mL) for 15 minutes at room temperature, a dichloromethane solution of Au(SMe$_2$)Cl (88.1 mg, 0.34 mmol in 5 mL CH_2Cl_2) was added dropwise in the dark, which resulted in the formation of a white precipitate. The resulting mixture was stirred at room temperature for an additional 2 h. Afterwards, the mixture was filtered through a plug of celite to remove the AgCl salt, and the residual solvent was removed under reduced pressure. The crude product was then collected and recrystallized from CH_2Cl_2/Et_2O to obtain the desired complex (105.1 mg, 0.24 mmol, 70% yield). ^{1}H NMR (DMSO-d_6, 300 MHz, 25 °C) δ 8.66 (d, J = 4.64 Hz, 1H, H^a), 8.53 (d, J = 7.24 Hz, 1H, H^e), 8.07 (t, J = 7.67 Hz, 1H, H^i), 7.79 (d, t, 2H, H^{c,d}), 7.08 (t, J = 7.85 Hz, 1H, H^f), 6.98 (t, J = 6.83 Hz, 1H, H^h), 2.14 (s, 3H, H^g). ^{13}C NMR (DMSO-d_6, 100.5 MHz, 25 °C): δ 178.1, 155.6, 152.9, 138.4, 137.9, 128.4, 127.4, 124.6, 123.4, 121.6, 118.6, 118.4, 12.4. Anal. calcd for $C_{13}H_{11}N_3AuCl$: C, 35.31; H, 2.49; N, 9.51%. Found: C, 35.20; H, 2.47; N, 9.47%.

4.1.4. Preparation of NHC–Au–Cl$_3$ complex 4. After dissolving complex **3** (200 mg, 0.45 mmol) in acetonitrile (10 mL) at room temperature, Au(SMe$_2$)Cl (235.9 mg, 0.91 mmol) was added, and the resulting mixture was stirred for an additional 5–6 h. Over time, the colourless solution turned yellow and was accompanied by the formation of a small amount of precipitate. The precipitate was presumed to be metallic gold and was subsequently collected and reused to synthesize Au(SMe$_2$)Cl. After filtration, the residual acetonitrile was removed under reduced pressure and at low temperature to obtain a yellow powder. The crude product was recrystallized from acetonitrile and diethyl ether to give the desired complex (76.1 mg, 0.15 mmol, 33% yield). ^{1}H NMR (DMSO-d_6, 300 MHz, 25 °C): δ 8.68 (d, J = 4.53 Hz, 1H, H^a), 8.47 (d, J = 7.21 Hz, 1H, H^e), 8.13 (t, J = 7.66 Hz, 1H, H^i), 7.86 (d, J = 7.7 Hz, 1H, H^d), 7.66 (t, 1H, H^c), 6.96 (t, J = 7.83 Hz, 1H, H^f), 6.82 (t, J = 6.80 Hz, 1H, H^h), 2.13 (s, 3H, H^g). ^{13}C NMR (DMSO-d_6, 100.5 MHz, 25 °C): δ 162.6, 146.8, 141.6, 130.8, 126.4, 125.9, 125.4, 125.0, 119.6, 119.0, 112.5, 110.6, 12.3. Anal. calcd for $C_{13}H_{11}N_3AuCl_3$: C, 30.43; H, 2.15; N, 8.19%. Found: C, 30.38; H, 2.11; N, 8.16%.

4.2. Crystal structure determination

Single crystals of **2** suitable for X-ray data collection were grown by the slow diffusion of diethyl ether into a saturated dichloromethane solution of the complex. The crystal data and details of the data collections for **2** are given in Table 1. X-ray data were collected on a CCD diffractometer with graphite monochromated Mo Kα radiation (k = 0.71073 Å) by use of ω scans. The structures were solved by direct methods and refined on F^2 using all reflections with the SHELX-97 program.[51] The nonhydrogen atoms were anisotropically refined. Hydrogen atoms that were not bound to imidazolium-C2 atoms were placed in calculated positions and assigned with an isotropic displacement parameter of 0.08 Å.

4.3. Cell culture assays

Cell lines, such as HCT-116 (human colorectal carcinoma), HepG2 (human hepatocellular carcinoma), A549 (human non-small lung carcinoma), and MCF-7 (human breast adenocarcinoma), were obtained from the National Centre for Cell Science, Pune, India. These cell lines were cultured in DMEM supplemented with 10% FBS and 1% antibiotic (PSN) and incubated at 37 °C in a humidified atmosphere with 5% CO_2. After achieving 75–80% confluence, cells were harvested with 0.025% trypsin and 0.52 mM EDTA in phosphate buffered saline (PBS) and were seeded a day before the start of experimentation at the desired density to allow them to re-equilibrate. All experiments were conducted in DMEM supplemented with 10% FBS and 1% antibiotic (PSN) solution.

4.4. Cell viability assays

Cells were treated with solutions of complexes **2**, **3**, or **4** (*i.e.*, at 0, 2.5, 5, 7.5, or 10 μM) for 24 h, dissolved in DMSO, suspended in DMEM media, and then their respective IC_{50} values were measured. In another set of experiments, cells were treated with cisplatin (0, 2.5, 5, 7.5, and 10 μM) for 24 h. The absorbance of the solubilized intracellular formazan was measured at 595 nm using an ELISA reader (Emax, Molecular Device, USA).

4.5. Assessment of cellular death parameters under a microscope

HepG2 cells treated with complex **3** at a pre-determined IC_{50} concentration for 24 h were viewed under a phase contrast microscope. The cells were also stained with 4′,6-diamidino-2-phenylindole (DAPI) for the detection of chromatin condensation and DNA fragmentation. The cells were observed under an inverted phase contrast/fluorescent microscope (Olympus IX70, Olympus Optical Co. Ltd., Shibuya-ku, Tokyo, Japan).

4.6. Detection of apoptosis using flow cytometry

Apoptosis was assayed *via* an annexin V-FITC apoptosis detection kit (Calbiochem, La Jolla, CA) as previously described.[48] HepG2 cells treated with complex **3** at a pre-determined IC_{50} concentration for 24 h were stained with PI and annexin V-FITC according to the manufacturer's instructions. The percentage of live, apoptotic, and necrotic cells were analyzed using a BD FACSVerse flow cytometer (Becton Dickinson, San Jose, CA, USA). The data from 10^4 cells were analyzed for each sample.

4.7. Analysis of cell cycle arrest

Cell cycle arrest was analyzed by treating HepG2 cells with complex **3** at a pre-determined IC_{50} concentration for 24 h followed by PI staining as previously described.[52] The percentages of the cell populations undergoing cell cycle arrest at various stages of cell division were analyzed using a BD LSRFortessa cell analyzer (Becton Dickinson, San Jose, CA, USA). The data from 10^4 cells were analyzed for each sample.

4.8. Caspase-3 and caspase-9 activity assay

HepG2 cells were treated with solutions of complex **3** (*i.e.*, at 0, 2.5, 5, 7.5, and 10 μM) dissolved in 0.05% v/v aq. DMSO for 24 h. The caspase-3 and caspase-9 activities were then quantified using a commercially available caspase-3/CPP32 and caspase-9 colorimetric assay kit (BioVision Research Products, Mountain View, CA), respectively, as previously described.[47] Caspase activities were spectrophotometrically measured at 405 nm using an ELISA reader (Model: Emax, Molecular Devices, USA).

4.9. Measurement of intracellular ROS upon treatment of HepG2 cells with complex 3

For the detection of intracellular ROS generation, the HepG2 cells were treated with complex **3** at a pre-determined IC_{50} concentration for 24 h and then incubated with 10 μM of 2′,7′-dichlorofluorescein diacetate (H_2DCFH-DA; Molecular Probes) for 25 min at 37 °C. The cells were then analyzed using a BD LSRFortessa cell analyzer. The data from 10^4 cells were analyzed for each sample.

4.10. Western blot analyses of protein expression in HepG2 cells following treatment with complex 3

Western blot analyses of the lysates of the cells treated with complex **3** (0, 2.5, and 5 μM) for 24 h were performed using 10–15% SDS-PAGE gels, primary antibodies, alkaline phosphatase-conjugated secondary antibodies, and NBT-BCIP as a chromogenic substrate as previously described.[53] Western blots facilitated the detection of PARP cleavage and the expression levels of procaspase-3, procaspase-9, cytosolic cytochrome c, Bax, and BCl-2. β-actin was used as a control.

Acknowledgements

This work was supported by grants from the Department of Science and Technology, DST, India under the SERC Fast Track Young Scientist Scheme (SR/FT/CS-046/2009). J.D. is grateful to Prof. R. D. Gupta and Prof. Y. Upadhyay, ITM University-Gwalior for their constant encouragement.

References

1 W. A. Herrmann and C. Kocher, *Angew. Chem., Int. Ed. Engl.*, 1997, **36**, 2162–2187.
2 L. Benhamou, E. Chardon, G. Lavigne, S. B. Laponnaz and V. Cesar, *Chem. Rev.*, 2011, **111**, 2705–2733.
3 A. J. Arduengo III, *Acc. Chem. Res.*, 1999, **32**, 913–921.
4 D. Puch and A. A. Danopoulos, *Coord. Chem. Rev.*, 2007, **251**, 610–641, and ref. therein.
5 B. M. Neilson and C. W. Bielawski, *J. Am. Chem. Soc.*, 2012, **134**, 12693–12699, and ref. therein.
6 A. S. K. Hashmi, A. M. Schuster and F. Rominger, *Angew. Chem., Int. Ed.*, 2009, **48**, 8247–8249.
7 S. Gaillard, M. Z. Slawin, A. T. Bonura, E. D. Stevens and S. P. Nolan, *Organometallics*, 2010, **29**, 394–402.
8 W. Liu and R. Gust, *Chem. Soc. Rev.*, 2013, **42**, 755–773.
9 F. Cisnetti and A. Gautier, *Angew. Chem., Int. Ed.*, 2013, **52**, 11976–11978.
10 L. Oehninger, R. Rubbiani and I. Ott, *Dalton Trans.*, 2013, **42**, 3269–3284.
11 A. Gautier and F. Cisnetti, *Metallomics*, 2012, **4**, 23–32.
12 M.-L. Teyssot, A.-S. Jarrousse, M. Manin, A. Chevry, S. Roche, F. Norre, C. Beaudoin, L. Morel, D. Boyer, R. Mahiou and A. Gautier, *Dalton Trans.*, 2009, 6894–6902.
13 B. Cetinkaya, E. Cetinkaya, H. Kucubay and R. Durmaz, *Arzneim.-Forsch./Drug Res.*, 1996, **46**, 821–823.
14 L. Meres and M. Albrecht, *Chem. Soc. Rev.*, 2010, **39**, 1903–1912.
15 J. C. Garrison and W. J. Youngs, *Chem. Rev.*, 2005, **105**, 3978–4008.
16 J. C. Y. Lin, R. T. W. Huang, C. S. Lee, A. Bhattacharyya, W. S. Hwang and I. J. B. Lin, *Chem. Rev.*, 2009, **109**, 3561–3598.
17 V. J. Catalano and M. A. Malwitz, *Inorg. Chem.*, 2003, **42**, 5483–5485.
18 J. T. Price, N. D. Jones and P. J. Ragogna, *Inorg. Chem.*, 2012, **51**, 6776–6783.
19 H. M. J. Wang and I. J. B. Lin, *Organometallics*, 1998, **17**, 972–975.
20 A. Kascatan-Nebioglu, M. J. Panzner, C. A. Tessier, C. L. Cannon and W. J. Youngs, *Coord. Chem. Rev.*, 2007, **251**, 884–895.

21 K. M. Hindi, T. J. Siciliano, S. Durmus, M. J. Panzner, D. A. Medvetz, D. V. Reddy, L. A. Hogue, C. E. Hovis, J. K. Hilliard, R. Mallett, C. A. Tessier, C. L. Cannon and W. J. Youngs, *J. Med. Chem.*, 2008, **51**, 1577–1583.
22 G. Roymahapatra, S. M. Mandal, W. F. Porto, T. Samanta, S. Giri, J. Dinda, O. L. Franco and P. K. Chattaraj, *Curr. Med. Chem.*, 2012, **19**, 4184–4193.
23 L. Messori and G. Marcon, *Met. Ions Biol. Syst.*, 2004, **41**, 279–304.
24 N. H. Kim, H. J. Park, M. K. Oh and I. S. Kim, *BMB Rep.*, 2013, **46**, 59–64.
25 C. F. Shaw III, *Chem. Rev.*, 1999, **99**, 2589–2600.
26 N. Marion, S. T. Díez-González and S. P. Nolan, *Angew. Chem., Int. Ed.*, 2007, **119**, 3046–3058.
27 P. J. Barnard and S. J. Berners-Price, *Coord. Chem. Rev.*, 2007, **2519**, 1889–1902.
28 S. Ray, R. Mohan, J. K. Singh, M. K. Samantaray, M. M. Shaikh, D. Panda and P. Ghosh, *J. Am. Chem. Soc.*, 2007, **129**, 15042–15053.
29 J. L. Hickey, R. A. Ruhayel, P. J. Barnerd, M. V. Baker, S. J. Berners-Price and A. Filipovska, *J. Am. Chem. Soc.*, 2008, **30**, 12570–12571.
30 T. Zou, C. T. Lum, S. Y. Chui and C.-M. Che, *Angew. Chem., Int. Ed.*, 2013, **52**, 2930–2933.
31 R. Rubbiani, S. Can, I. Kitanovic, H. Alborzinia, M. Stefanopoulou, M. Kokoschka, S. Mönchgesang, W. S. Sheldrick, S. Wölfl and I. Ott, *J. Med. Chem.*, 2011, **54**, 8646–8657.
32 S. J. Berners-Price, *Angew. Chem., Int. Ed.*, 2011, **50**, 804–805.
33 L. Oehninger, R. Rubbiani and O. Ingo, *Dalton Trans.*, 2013, **42**, 3269–3284.
34 (*a*) D. Fan, C. T. Yang, J. D. Ranford, P. F. Lee and J. J. Vittal, *J. Chem. Soc., Dalton Trans.*, 2003, 2680; (*b*) D. Fan, C.-T. Yang, J. D. Ranford, J. J. Vittal and P. F. Lee, *Dalton Trans.*, 2003, 3376–3381.
35 R. Cao, J. Jia, X. Ma, M. Zhou and H. Fei, *J. Med. Chem.*, 2013, **56**, 3636–3644.
36 S. D. Adhikary, D. Bose, P. Mitra, K. D. Saha, V. Bertolasi and J. Dinda, *New J. Chem.*, 2012, **36**, 759–767.
37 T. Samanta, B. K. Rana, G. Roymahapatra, S. Giri, P. Mitra, R. Pallepogu, P. K. Chattaraj and J. Dinda, *Inorg. Chim. Acta*, 2011, **375**, 271–279.
38 J. Dinda, S. D. Adhikary, S. K. Seth and A. Mahapatra, *New J. Chem.*, 2013, **37**, 431–438.
39 S. Gaillard, M. Z. Slawin, A. T. Bonura, E. D. Stevens and S. P. Nolan, *Organometallics*, 2010, **29**, 394–402.
40 P. Frémont, R. Singh, E. D. Stevens, J. L. Peterson and S. P. Nolan, *Organometallics*, 2007, **26**, 1376–1385.
41 C. G. Hartinger, N. Metzler-Nolte and P. J. Dyson, *Organometallics*, 2012, **31**, 5677–5685.
42 P. J. Barnard and S. J. Berners-Price, *Coord. Chem. Rev.*, 2007, **251**, 1889–1902.
43 H. G. Raubenheimer and S. Cronje, *Chem. Soc. Rev.*, 2008, **37**, 1998–2011.
44 M. Pellei, V. Gandin, M. Marinelli, C. Marzano, M. Yousufuddin, H. V. Dias and C. Santini, *Inorg. Chem.*, 2012, **51**, 9873–9882.
45 S. K. Dey, D. Bose, A. Hazra, S. Naskar, A. Nandy, R. N. Munda, S. Das, N. Chatterjee, N. B. Mondal, S. Banerjee and K. D. Saha, *PLoS One*, 2013, **8**, e58055.
46 J. Dinda, T. Samanta, A. Nandy, K. Das Saha, S. K. Seth, S. K. Chattopadhyay and C. W. Bielawski, *New J. Chem.*, 2014, **38**, 1218–1224.
47 S. Mallick, B. C. Pal, J. R. Vedasiromoni, D. Kumar and K. D. Saha, *Cell. Physiol. Biochem.*, 2012, **30**, 915–926.
48 A. Nandy, S. K. Dey, S. Das, R. N. Munda, J. Dinda and K. D. Saha, *Mol. Cancer*, 2014, **13**, 1–14.
49 B. K. Rana, A. Nandy, V. Bertolasi, C. W. Bielawski, K. D. Saha and J. Dinda, *Organometallics*, 2014, **33**, 2544–2548.
50 R. Uson, A. Laguna and M. Laguna, *Inorg. Synth.*, 1989, **26**, 85–91.
51 G. M. Sheldrick, *SHELX-97, Program for Crystal Structure Refinement*, University of Gottingen, Germany, 1997.
52 S. Mallick, P. Ghosh, S. K. Samanta, S. Kinra, B. C. Pal, A. Gomes and J. R. Vedasiromoni, *Cancer Chemother. Pharmacol.*, 2010, **66**, 709–719.
53 S. Das, N. Chatterjee, D. Bose, S. K. Dey, R. N. Munda, A. Nandy, S. Bera, S. K. Biswas and K. D. Das, *Cell. Physiol. Biochem.*, 2012, **29**, 251–260.

